Physics Letters A 377 (2013) 1925–1929

Contents lists available at SciVerse ScienceDirect

Physics Letters A

www.elsevier.com/locate/pla

# Carrier dependent ferromagnetism in chromium doped topological insulator $Cr_y(Bi_xSb_{1-x})_{2-y}Te_3$

Bin Li, Qingyan Fan, Fuhao Ji, Zhen Liu, Hong Pan, S. Qiao *

*Department of Physics, State Key Laboratory of Surface Physics, and Laboratory of Advanced Materials, Fudan University, Shanghai 200433, People's Republic of China*

ARTICLE INFO

*Article history:*
Received 8 January 2013
Received in revised form 4 May 2013
Accepted 10 May 2013
Available online 15 May 2013
Communicated by R. Wu

*Keywords:*
Topological insulator
Ferromagnetism
AHE
RKKY interaction

ABSTRACT

To understand the mechanism of ferromagnetism in topological insulator, we studied the structural, magnetic and transport characters of $Cr_y(Bi_xSb_{1-x})_{2-y}Te_3$ single crystals. The Curie temperature $T_C$, which is determined from magnetization and anomalous Hall effect (AHE) measurements by Arrott plots, is found to be proportional to $y_{Cr} * p^{1/3}$, where $p$ is the hole density. This fact supports a scenario of Ruderman–Kittel–Kasuya–Yoshida (RKKY) interaction with mean-field approximation.



## 1. Introduction

Topological insulators (TIs) are promising candidates of spintronics materials because of their robust helical surface states and the extremely strong spin–orbit interaction [1–3]. Initially, binary chalcogenides $Bi_2Te_3$, $Sb_2Te_3$ and $Bi_2Se_3$ have been identified as three-dimensional TIs by surface sensitive probes such as angle resolved photoemission spectroscopy and scanning tunneling microscopy/spectroscopy. Later, ternary chalcogenide $(Bi_xSb_{1-x})_2Te_3$ [4,5], which has similar tetradymite structure to the parent compounds $Bi_2Te_3$ and $Sb_2Te_3$, was predicted by ab initio calculations and confirmed by ARPES measurements as a tunable topological



magnetism or superconductivity, TIs have attracted great attention due to the rich variety of new physics and applications. The ferromagnetism in several transition metal (TM) doped TIs, which breaks the time-reversal symmetry, has been reported [6–13]. Ferromagnetism in TIs is important because the combination of magnetism with TIs makes a good platform to study fundamental physical phenomena, such as the quantum anomalous Hall effect [14–17], Majorana fermions [18], image magnetic monopole effect [19], and topological contributions to the Faraday and Kerr magneto-optical effect [20].

Recently, it has been proposed that uniformly deposited magnetic atoms on the surface of TIs could naturally result in the ferromagnetic phase through RKKY interactions [21,22]. These long-range spin–spin interactions mediated by helical massless itinerant electrons, which is the characteristic of TI, would lead to the surface magnetism [22,23]. Besides, the surface long-range magnetic order is expected to be stronger than bulk because RKKY interaction is inversely proportional to the gap, which is small for the surface and large for the bulk. So there is a regime $T_C^{bulk} <$

attracted attention because it is the system that shows the largest AHE until now. Another distinctive character of this system is the carrier-independent ferromagnetism which conflicts with the carrier-mediated mechanism of ferromagnetism in dilute magnetic semiconductor (DMS) [25–28]. In current theory, the ferromagnetic exchange interactions between local magnetic moments of dilute magnetic atoms is mediated by itinerant carriers, so the interaction and $T_C$ are strongly dependent on the distance between magnetic atoms and the density of charge carriers, and the study on the mechanism of carrier-independent ferromagnetism is an important task. To carry out this task, the territory of the special character must be clarified. If it is surface state related, then it may be related to the unique massless helical topological surface state of TI.

* Corresponding author. Tel.: +86 21 51630254.
*E-mail address:* qiaoshan@fudan.edu.cn (S. Qiao).

0375-9601 
http://dx.doi.org/10.1016/j.physleta.2013.05.020

Although the magnetic characters of $Sb_{2-x}Cr_xTe_3$ crystals grown by Bridgman technique [11] and films [12] have been reported, the studies focused on the change of magnetic properties on Cr concentrations. To check if the carrier-independent ferromagnetism also exists in bulk states of Cr-doped $(Bi_xSb_{1-x})_2Te_3$, the study on different carrier density is important.

In this work, to overcome the problems mentioned above, we made use of uniform high temperature sintering method to prepare single crystals with stable uniform Cr distribution and adjusting Bi/Sb ratio to control the carrier density. The structural, magnetic and magneto-transport properties are investigated and clear AHE indicates the existence of intrinsic bulk ferromagnetism. $T_C$ is found to be proportional to $y_{Cr} * p^{1/3}$, which shows that their bulk magnetic properties can be explained by holes-mediated RKKY mechanism.

## 2. Experiments

Single crystals were synthesized by melting stoichiometric amounts of high-purity elemental Bi (99.999%), Te (99.999%), Sb (99.9999%) and Cr (99.95%) in sealed evacuated quartz glass tube at 800 °C for 17 hours, and then slowly cooled down to 550 °C in a 24 hours period, and finally naturally cooled to room temperature. The obtained crystals were easily cleaved along the plane with shiny flat surface. The actual Cr concentrations $y$ in $Cr_y(Bi_xSb_{1-x})_{2-y}Te_3$ ($x = 0, 0.15, 0.20, 0.25, 0.35, 0.50$; $y \approx 0.050$), which were determined by inductively coupled plasma (ICP) measurements, are almost the same in the samples with different Bi contents. The powder X-ray diffraction (XRD) experiments were carried out at beamline 14B1 of Shanghai Synchrotron Radiation Facility (SSRF), with photon wavelength 1.2385 Å, and divergence angle $2.5 * 0.15$ mrad$^2$ in horizontal and vertical directions. The MDI Jade 5.0 software was used to analyze the data. Single crystals were used for the observation of magnetic properties using the superconducting quantum interference device (SQUID) magnetometer from Quantum Design. Exfoliated thin flakes of about 85–180 nm thickness on $SiO_2$ were used for magneto-transport experiments by physical property measurement system (PPMS) from Quantum Design. Both the measurements of temperature dependent longitudinal resistivity $\rho_{xx}(T)$ and Hall resistivity $\rho_{xy}$ were carried out in PPMS using the van der Pauw method and the current was perpendicular to the $c$ axis. Because the estimation of $T_C$ by the appearance of hysteresis or non-zero remnant magnetization is not accurate, the criterion of Arrott plots [29] is used here to minimize the effects of magnetic anisotropy and domain rotation. In Arrott plots, $H/M$ versus $M^2$ should go as $H/M = a'(T - T_C) + b'M^2 + c'M^4$ when $H$ is above coercivity. A positive or negative slope indicates a second-order or first-order transition respectively and the intercept changes sign at $T_C$.

## 3. Results and discussion

### 3.1. Structure analysis

To study the crystal structure, XRD measurements were carried out. According to XRD patterns shown in Fig. 1(a), all peaks of $Cr_{0.05}Sb_{1.95}Te_3$ appear in that of $Cr_y(Bi_xSb_{1-x})_{2-y}Te_3$ ($x = 0.15, 0.25, 0.50$) samples, indicating that the Bi doping did not change the crystal structure. To get the lattice constants precisely, two steps are taken to process the data. First determine the locations of peaks by profile fitting, and then refine the lattice constants. The profile fittings are done with linear background in segments, in which Pearson-VII function is used and skewness is set to be zero. The peak locations are used in the cell refinement after the weak peaks and strong overlapping peaks are removed. The obtained lattice parameters $a$ and $c$ are presented in Fig. 1(b). The

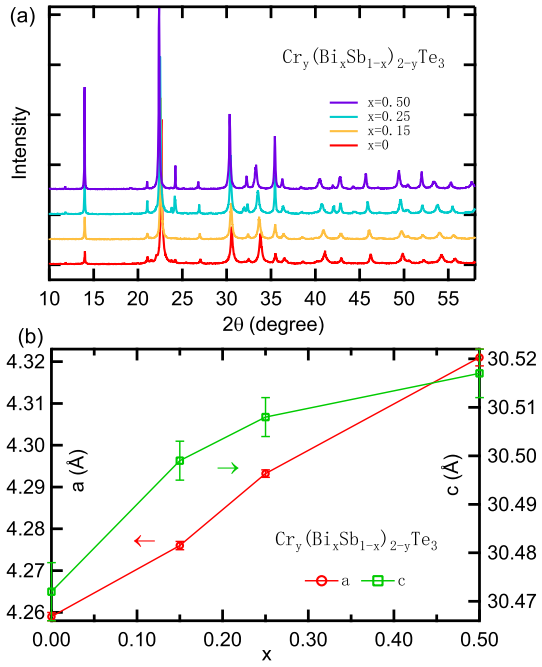


**Fig. 1.** (Color online.) XRD patterns (a) and the lattice constants $a$ and $c$ (b) of $Cr_y(Bi_xSb_{1-x})_{2-y}Te_3$ as a function of the Bismuth concentration $x$.

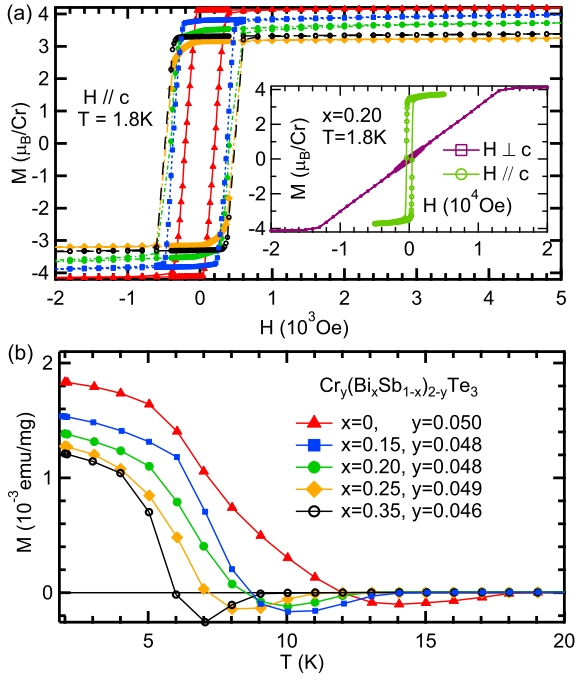


**Fig. 2.** (Color online.) Magnetization of $Cr_y(Bi_xSb_{1-x})_{2-y}Te_3$ crystals. (a) The $M(H)$ curves measured at 1.8 K with $H$ // $c$ and the inset shows the anisotropy of $Cr_{0.048}(Bi_{0.2}Sb_{0.8})_{1.952}Te_3$ crystal. (b) The corresponding temperature dependence of remnant magnetization after saturated magnetization with 5 kOe $H$ // $c$ at 1.8 K.

lattice constants $a$ and $c$ rise with the increase of Bi concentration, showing the smooth substitution of Bi for Sb which can in turn lift up the Fermi level $E_F$ as reported [4–6].

### 3.2. Magnetic properties

The inset of Fig. 2(a) shows the anisotropy of $Cr_{0.048}(Bi_{0.2}Sb_{0.8})_{1.952}Te_3$ crystal. Compared with the $M(H)$ loop for $H \perp c$, the sharp, nearly square hysteresis loops with small coercivity for $H$ // $c$ indicate the existence of ferromagnetism with

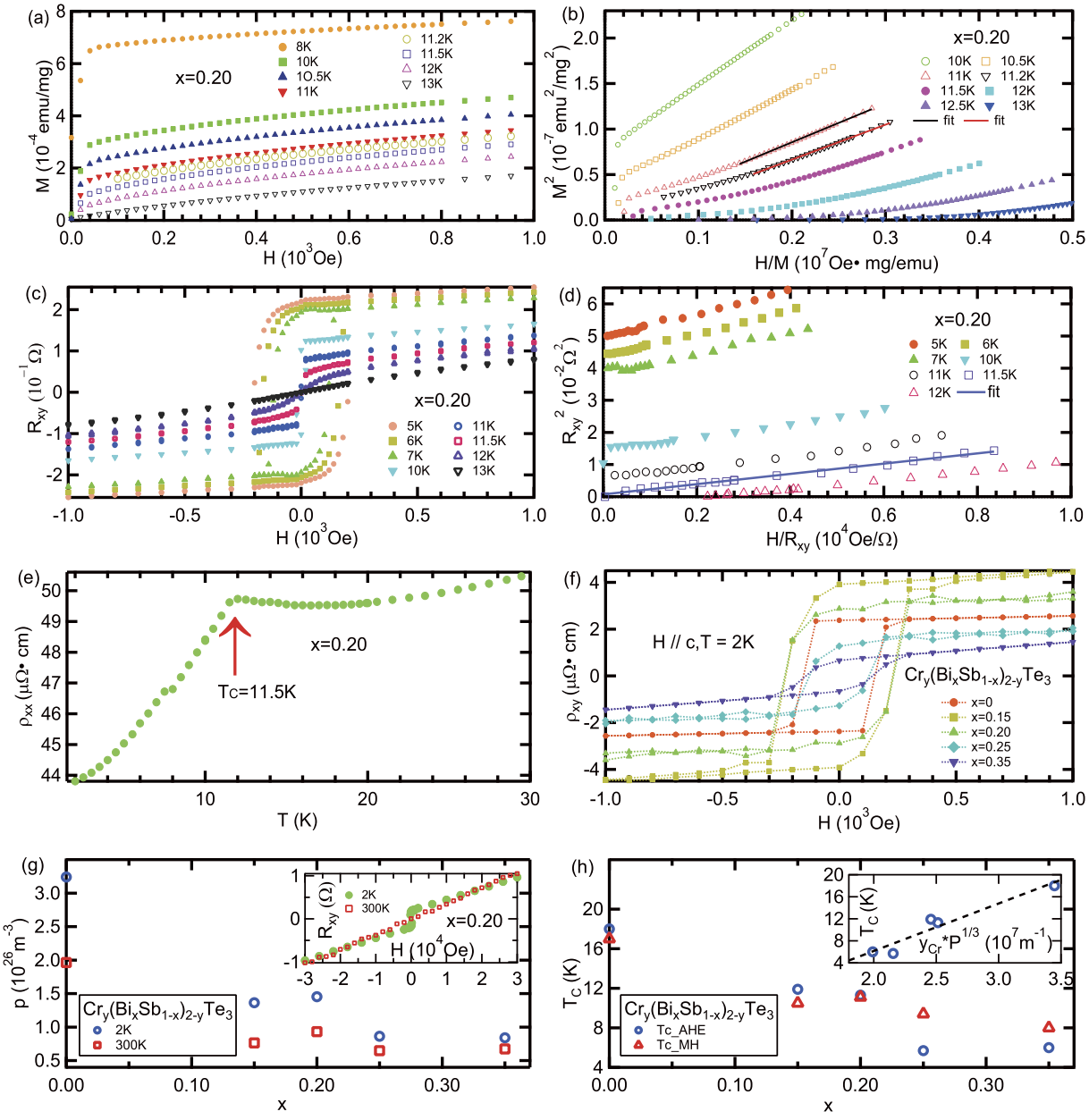


**Fig. 3.** (Color online.) Magneto-transport properties of $Cr_y(Bi_xSb_{1-x})_{2-y}Te_3$ crystals. (a) The $M(H)$ isotherms and (b) its corresponding Arrott plots for $x = 0.20$ with $H \,//\, c$. (c) The $R_{xy}$ isotherms and (d) its corresponding Arrott plots for $x = 0.20$ with $H \,//\, c$. (e) Longitudinal electrical resistivity $\rho_{xx}(T)$ for $x = 0.20$. (f) Hall resistivity $\rho_{xy}(H)$ measured at 2 K for $Cr_y(Bi_xSb_{1-x})_{2-y}Te_3$ ($x = 0, 0.15, 0.20, 0.25, 0.35$), and dashed is the guide line. (g) The carrier densities at 2 K and 300 K of all samples. Inset: Long range $R_{xy}(H)$ curve for $x = 0.20$ at 2 K and 300 K. (h) Curie temperature $T_C$ with different bismuth concentration $x$. Inset: Relation between $T_C$ and $y_{Cr} * p^{1/3}$ at 2 K with the theoretical fitting based on RKKY interaction.

the easy magnetization axis perpendicular to the sample surface. Fig. 2(a) represents the magnetization vs. magnetic field curves of $Cr_y(Bi_xSb_{1-x})_{2-y}Te_3$ ($x = 0, 0.15, 0.20, 0.25, 0.35$) at 1.8 K. The small coercivity of about 400 Oe, much smaller than that of 12 kOe at 2 K for V-doped $Sb_2Te_3$ [10], indicates the magnetic softness of the samples. The saturated magnetic moment is 3.464 $\mu_B$ per Cr atom for $x = 0.20$, which is consistent with Hund rule for $Cr^{3+}$ ion with $3d^3$ electron configuration after considering the quench of orbit moment owing to the crystal field.

The corresponding temperature dependences of remnant magnetization $M(T)$ after 5 kOe saturated magnetization at 1.8 K along $c$ axis are shown in Fig. 2(b) and $T_C$ can be roughly estimated from these $M(T)$ curves.

The $M(H)$ isotherms and its corresponding Arrott plots of a typical sample, $Cr_{0.048}(Bi_{0.2}Sb_{0.8})_{1.952}Te_3$, in the vicinity of its $T_C$ are presented in Fig. 3(a) and Fig. 3(b), respectively, which indicates that the ferromagnetic transition in $Cr_{0.048}(Bi_{0.2}Sb_{0.8})_{1.952}Te_3$ is of second order as expected, with $T_C$ determined as 11.1 K.

### 3.3. Magneto-transport properties

Transport measurements were performed for samples with different Bi concentrations and similar results were obtained. Fig. 3(c)–(e) and the inset of Fig. 3(g) show the results of typical $Cr_{0.048}(Bi_{0.2}Sb_{0.8})_{1.952}Te_3$ sample and Fig. 3(f)–(h) show the results of all $Cr_y(Bi_xSb_{1-x})_{2-y}Te_3$ samples with different $x$.

AHE is a commonly observed phenomenon in ferromagnetic materials caused by spin–orbit interactions, which can be very sensitive to the Berry phase determined by band structure [30]. It is well known that in ferromagnetic materials the Hall resistivity can

be expressed as a sum of two contributions, $\rho_{xy} = \rho_H + \rho_{AH} = R_0 H + R_A M = R_{xy}/d$, where $R_0$ and $R_A$ are the ordinary and the anomalous Hall coefficients, respectively; $H$ is the applied magnetic field; $M$ is the magnetization; $d$ is the thickness of the sample. Anomalous Hall resistivity $\rho_{AH}$ can be deduced by subtracting the ordinary Hall resistivity $\rho_H$ from $\rho_{xy}$. In practice, $\rho_{xy}^{exp}$ contains both longitudinal and Hall contributions, and here the pure Hall contribution $\rho_{xy}$ is extracted from experimental data by the difference of $\rho_{xy}^{exp}$ for positive and negative field directions: $\rho_{xy} = [\rho_{xy}^{exp}(+H) - \rho_{xy}^{exp}(-H)]/2$. This process can remove the $\rho_{xx}$ due to the misalignment of electrodes, because the background $\rho_{xx}$ is usually symmetric with $H$.

The $R_{xy}$ of $Cr_{0.048}(Bi_{0.2}Sb_{0.8})_{1.952}Te_3$ at different temperatures are shown in Fig. 3(c). If the ferromagnetism is resulted from magnetic clusters or phase segregation, the hysteresis loops, namely AHE, cannot be observed, thus further unambiguously confirm the ferromagnetism is intrinsic. Because Hall resistance $R_{xy}$ reflects magnetization $M$ of ferromagnetic materials, the Arrott plots can also be obtained from $R_{xy}$ measurements. Fig. 3(d) shows the Arrott plots deduced from the data shown in Fig. 3(c), in which $R_{xy}^2$ is plotted against $H/R_{xy}$ at each temperature and the extrapolated intercept is proportional to the saturation magnetization $M_s$. $T_C$ is determined as 11.5 K by searching the isotherm with zero intercept, almost the same as that determined by SQUID magnetization measurements shown in Fig. 3(b).

Fig. 3(e) shows the longitudinal resistivity $\rho_{xx}(T)$ of $Cr_{0.048}(Bi_{0.2}Sb_{0.8})_{1.952}Te_3$. $\rho_{xx}(T)$ displays a maximum at about 11.5 K, which is just $T_C$, suggesting a paramagnetic to ferromagnetic phase transition here. The similar features have been observed in other DMS, such as $Sb_{2-x}V_xTe_3$ [10], and can be explained by magnetic impurity scattering due to the enhanced magnetic fluctuation around magnetic ions near $T_C$. Besides, $\rho_{xx}(T)$ shows a metallic character at the temperature range in paramagnetic phase. Compared with magnetization measurements that cannot exclude local effects, magneto-transport measurements provide the results averaged over the entire sample. Thus the appearance of peak in longitudinal electrical resistivity $\rho_{xx}$ and clear AHE strongly support the presence of broad intrinsic ferromagnetic phase below $T_C$. The $\rho_{xy}$ of $Cr_y(Bi_xSb_{1-x})_{2-y}Te_3$ ($x = 0, 0.15, 0.20, 0.25, 0.35$) at 2 K are shown in Fig. 3(f) and clear AHE can be observed for all samples.

In order to determine the carrier type and density, the ordinary Hall coefficient $R_0$ is determined by the slope of the linear part of $\rho_{xy}$ curve at high magnetic field range. The three-dimensional (3D) hole density $p$ is calculated as $p = e/R_0$, where $e$ is the elementary charge. The inset of Fig. 3(g) shows the long-range $R_{xy}(H)$ curve of $Cr_{0.048}(Bi_{0.2}Sb_{0.8})_{1.952}Te_3$, and the carrier density can be deduced as $1.45 \times 10^{26}$ m$^{-3}$ at 2 K and $9.3 \times 10^{25}$ m$^{-3}$ at 300 K, which are ascribed to the presence of a large number of native anti-site defects. For all samples, positive slopes are observed, which reflect the $p$-type charge carrier. Fig. 3(g) shows the density of holes $p$ of $Cr_y(Bi_xSb_{1-x})_{2-y}Te_3$ at 2 K and 300 K, in which $p$ decreases with the increase of Bi concentration $x$, corresponding to the rise of Fermi level $E_F$ as reported [4–6].

### 3.4. Ferromagnetism mechanism

In DMS [25], the density of magnetic impurities is very low compared to the host atoms, thus these magnetic impurities are far apart which makes the direct coupling between them impossible, so the only interaction which can result in ferromagnetism should be carrier induced via indirect coupling. RKKY interaction is the most famous model dealing with long-range indirect coupling. In RKKY model [26], a localized magnetic moment spin-polarizes the conduction electrons and this polarization in turn couples to neighborly localized moments. The interaction is long range and has an oscillatory dependence on the distance between the magnetic moments and can be either ferromagnetic or antiferromagnetic depending on the separation of the two ions. For a DMS with a typical carrier density, the period of this oscillation becomes very large, and the first zero of the oscillation falls at a distance greater than the cut-off length of the indirect exchange interaction. In this case, the RKKY interaction under the mean-field approximation degenerates into the Zener model [27]. The interaction is mediated by carriers, and the carrier density determines the strength of exchange interaction and $T_C$ is proportional to $J^2 m^* k_F$ where $k_F = (3\pi^2 p)^{1/3}$ [28].

Fig. 3(h) summarizes the correlation between bismuth concentration $x$ and $T_C$. It's clearly seen that $T_C$ is decreased with increase of $x$. From the dependence of holes concentration $p$ on $x$ at 2 K temperature shown in Fig. 3(g), the relationship between $T_C$ and $y_{Cr} * p^{1/3}$ can be established as shown in the inset of Fig. 3(h) and can be fitted by $T_C \sim y_{Cr} * p^{1/3}$, which supports that the RKKY interaction is responsible for the ferromagnetism in $Cr_y(Bi_xSb_{1-x})_{2-y}Te_3$ crystals. The carrier-independent ferromagnetism in $Cr_{0.22}(Bi_xSb_{1-x})_{1.78}Te_3$ ultrathin films is explained by the enhanced van Vleck paramagnetism with a band origin [6,16], which conflicts with the carrier-mediated mechanism of ferromagnetism in DMS. From our results, $T_C$ of $Cr_y(Bi_xSb_{1-x})_{2-y}Te_3$ crystals are carrier dependent and obey the RKKY mechanism, so the carrier-independent ferromagnetism in ultrathin films may be related to the surface states of TI. Besides, $T_C$ of crystals is lower than that of the ultrathin films, which is in accordance with the theoretical prediction [24] that $T_C$ of surface magnetism could be higher than that of the bulk TI. With high enough sensitivity, the observation of such higher $T_C$ would be possible. But in our experiments, no double $T_C$ values were detected because both the Hall effect and SQUID measurements are bulk sensitive. The Hall resistance of $Cr_{0.22}Sb_{1.78}Te_3$ film with 5 nm thickness is about 148 ohm [6], so the Hall resistance $R_S$ of surface state should be larger than 148 ohms. The Hall resistance $R_B$ of our sample with 85 nm thickness is 0.27 ohm. Because the ratio of $R_B/R_S$ is about 0.18%, so the surface contribution can only be seen when the error of Hall effect measurement is below 0.18%. The error of our Hall effect measurements is larger than 2%, so the Hall effect signal related to surface state cannot be detected in our measurements.

If the thickness of the sample is thick enough that the bulk ferromagnetism dominates, and thin enough that the carrier density can be adjusted by gate voltage [22,23,25], the carrier-dependent ferromagnetism enables the possibility to control the magnetic properties by gate voltage in the future scientific researches and spintronics applications [22,25,31,32].

## 4. Conclusion

In summary, ferromagnetic ordering in $Cr_y(Bi_xSb_{1-x})_{2-y}Te_3$ crystal is observed by magnetization and magneto-transport measurements. The Curie temperature $T_C$ is found to depend on hole density and can be explained by a scenario of RKKY interaction. The results also imply that the magnetic coupling mechanisms in surface and bulk ferromagnetism of $Cr_{0.22}(Bi_xSb_{1-x})_{1.78}Te_3$ are different.

Note that, this work was first reported online on arXiv:1207.4363 on 18 July 2012 and was done parallel with the similar work by H. Li et al. published in Appl. Phys. Lett. 101 (2012) 072406.

## Acknowledgements

We acknowledge the technical support and help from stuff members of BL14B1 beamline in SSRF during the XRD measurements. This work is supported by the Natural Science Foundation of China (Nos.: 10979021, 11027401, and 11174054), the Ministry

of Science and Technology of China (National Basic Research Program No. 2011CB921800) and Shanghai Municipal Education Commission.

## References


[1] M.Z. Hasan, C.L. Kane, Rev. Mod. Phys. 82 (2010) 3045.
[2] X.L. Qi, S.C. Zhang, Phys. Today 63 (2010) 33;
X.L. Qi, S.C. Zhang, Rev. Mod. Phys. 83 (2011) 1057.
[3] Haijun Zhang, Chao-Xing Liu, Xiao-Liang Qi, Xi Dai, Zhong Fang, Shou-Cheng Zhang, Nature Phys. 5 (2009) 438.
[4] Desheng Kong, Yulin Chen, Judy J. Cha, Qianfan Zhang, James G. Analytis, Keji Lai, Zhongkai Liu, Seung Sae Hong, Kristie J. Koski, Sung-Kwan Mo, Zahid Hussain, Ian R. Fishe, Zhi-Xun Shen, Yi Cui, Nature Nano. 6 (2011) 705, http://dx.doi.org/10.1038/nnano.2011.172.
[5] Jinsong Zhang, Cui-Zu Chang, Zuocheng Zhang, Jing Wen, Xiao Feng, Kang Li, Minhao Liu, Ke He, Lili Wang, Xi Chen, Qi-Kun Xue, Xucun Ma, Yayu Wang, Nature Commun. 2 (2011) 574, http://dx.doi.org/10.1038/ncomms1588.
[6] Cui-Zu Chang, Jin-Song Zhang, Min-Hao Liu, Zuo-Cheng Zhang, Xiao Feng, Kang Li, Li-Li Wang, Xi Chen, Xi Dai, Zhong Fang, Xiao-Liang Qi, Shou-Cheng Zhang, Yayu Wang, Ke He, Xu-Cun Ma, Qi-Kun Xue, Adv. Mater. 25 (2013) 1065;
Cui-Zu Chang, et al., Science 339 (2013) 1582.
[7] Y.L. Chen, J.-H. Chu, J.G. Analytis, Z.K. Liu, K. Igarashi, H.-H. Kuo, X.L. Qi, S.K. Mo, R.G. Moore, D.H. Lu, M. Hashimoto, T. Sasagawa, S.C. Zhang, I.R. Fisher, Z. Hussain, Z.X. Shen, Science 329 (2010) 659.
[8] L. Andrew Wray, Su-Yang Xu, Yuqi Xia, David Hsieh, Alexei V. Fedorov, Yew San Hor, Robert J. Cava, Arun Bansil, Hsin Lin, M. Zahid Hasan, Nature Phys. 7 (2011) 32.
[9] Y.S. Hor, P. Roushan, H. Beidenkopf, J. Seo, D. Qu, J.G. Checkelsky, L.A. Wray, D. Hsieh, Y. Xia, S.-Y. Xu, D. Qian, M.Z. Hasan, N.P. Ong, A. Yazdani, R.J. Cava, Phys. Rev. B 81 (2010) 195203.
[10] J.S. Dyck, Pavel Hájek, Petr Lošťák, Ctirad Uher, Phys. Rev. B 65 (2002) 115212; Zhenhua Zhou, Yi-Jiunn Chien, Ctirad Uher, Appl. Phys. Lett. 87 (2005) 112503.
[11] J.S. Dyck, Č. Drašar, P. Lošťák, C. Uher, Phys. Rev. B 71 (2005) 115214.
[12] Zhenhua Zhou, Yi-Jiunn Chien, Ctirad Uher, Phys. Rev. B 74 (2006) 224418.
[13] V.A. Kulbachinskiĭ, P.M. Tarasov, E. Brük, JETP Lett. 73 (2001) 352.
[14] F.D.M. Haldane, Phys. Rev. Lett. 61 (1988) 2015.
[15] C.X. Liu, X.L. Qi, X. Dai, Z. Fang, S.C. Zhang, Phys. Rev. Lett. 101 (2008) 146802.
[16] R. Yu, W. Zhang, H.J. Zhang, S.C. Zhang, X. Dai, Z. Fang, Science 329 (2010) 61.
[17] K. Nomura, N. Nagaosa, Phys. Rev. Lett. 106 (2011) 166802.
[18] Liang Fu, C.L. Kane, Phys. Rev. Lett. 100 (2008) 096407;
Marcel Franz, Physics 3 (2010) 24;
Jason Alicea, Phys. Rev. B 81 (2010) 125318;
Titus Neupert, Shigeki Onoda, Akira Furusaki, Phys. Rev. Lett. 105 (2010) 206404.
[19] X.L. Qi, R. Li, J. Zang, S.C. Zhang, Science 323 (2009) 1184.
[20] X.L. Qi, T.L. Hughes, S.C. Zhang, Phys. Rev. B 78 (2008) 195424.
[21] Qin Liu, Chao-Xing Liu, Cenke Xu, Xiao-Liang Qi, Shou-Cheng Zhang, Phys. Rev. Lett. 102 (2009) 156603.
[22] I. Garate, M. Franz, Phys. Rev. Lett. 104 (2010) 146802;
I. Garate, M. Franz, Phys. Rev. B 81 (2010) 172408.
[23] J.J. Zhu, D.X. Yao, S.C. Zhang, K. Chang, Phys. Rev. Lett. 106 (2011) 097201.
[24] G. Rosenberg, M. Franz, Phys. Rev. B. 85 (2012) 195119.
[25] H. Ohno, Science 281 (1998) 951;
H. Ohno, J. Magn. Magn. Mater. 200 (1999) 110;
H. Ohno, D. Chiba, F. Matsukura, T. Omiya, E. Abe, T. Dietl, Y. Ohno, K. Ohtani, Nature 408 (2000) 944;
T. Dietl, Nat. Mater. 9 (2010) 965.
[26] T. Dietl, A. Haury, Y. Merle d'Aubigné, Phys. Rev. B 55 (1997) R3347.
[27] C. Zener, Phys. Rev. 81 (1950) 440;
T. Dietl, H. Ohno, F. Matsukura, J. Cibert, D. Ferrand, Science 287 (2000) 1019.
[28] T. Jungwirth, K.Y. Wang, J. Mašek, K.W. Edmonds, Jürgen König, Jairo Sinova, M. Polini, N.A. Goncharuk, A.H. MacDonald, M. Sawicki, A.W. Rushforth, R.P. Campion, L.X. Zhao, C.T. Foxon, B.L. Gallagher, Phys. Rev. B 72 (2005) 165204.
[29] A. Arrott, Phys. Rev. 108 (1957) 1394;
A. Arrott, J. Noakes, Phys. Rev. Lett. 19 (1967) 786.
[30] N. Nagaosa, J. Sinova, S. Onoda, A.H. MacDonald, N.P. Ong, Rev. Mod. Phys. 82 (2010) 1539.
[31] T. Yokoyama, Y. Tanaka, N. Nagaosa, Phys. Rev. B 81 (2010) 121401(R).
[32] Joseph Maciejko, Eun-Ah Kim, Xiao-Liang Qi, Phys. Rev. B 82 (2010) 195409.